J Intell Robot Syst (2011) 63:115–129
DOI 10.1007/s10846-010-9498-4

Obstacle-Free Pathway Detection by Means of Depth Maps

Nuria Ortigosa · Samuel Morillas · Guillermo Peris-Fajarnés

Received: 2 February 2009 / Accepted: 18 October 2010 / Published online: 3 November 2010

Abstract The detection of surrounding obstacle-free space is an essential task for many intelligent automotive and robotic applications. In this paper we present a method to detect obstacle-free pathways in real-time using depth maps from a pair of stereo images. Depth maps are obtained by processing the disparity between left and right images from a stereo-vision system. The proposed technique assumes that depth of pixels in obstacle-free pathways should increase slightly and linearly from the bottom of the image to the top. The proposed real-time detection checks whether the depth of groups of image columns matches a linear model. Only pixels fulfilling the matching requirements are identified as obstacle-free pathways. Experimental results with real outdoor stereo images show that the method performance is promising.

Keywords Assisted navigation · Pathway detection · Depth map · Obstacle-free space

1 Introduction

During last years, obstacle-free space detection has been researched by many authors, specially for intelligent automotive and robotic applications, in order to aid automotive navigation without collisions. Thus, in order to help navigation, there are authors who detect and classify obstacles [1] or detect the painted lane markings [2].

N. Ortigosa (✉) · G. Peris-Fajarnés
Centro de Investigación en Tecnologías Gráficas, Universidad Politécnica de Valencia, Camino de Vera s/n, 46022 Valencia, Spain
e-mail: nuorar@upvnet.upv.es

S. Morillas
Instituto Universitario de Matemática Pura y Aplicada, Universidad Politécnica de Valencia, Camino de Vera s/n, 46022 Valencia, Spain

A general overview in [3] differences between those methods based on active sensors and the ones which use passive sensors to acquire data from the environment.

Active sensors, such as radar-based, laser-based, and acoustic-based detect the distance of objects by measuring the travel time of a signal emitted by the sensors and reflected by the objects. A Lidar ("Light Detection and Ranging") also transmits and receives electromagnetic radiation, but at a higher frequency. In this field, [4] detects free space around the robot, [5] uses laser and radar systems to detect vehicles, [6] detects topological structure of the environment by means of a number of laser range finders and [7] and [8] use sonar for obstacle avoidance.

Optical sensors, such as normal cameras, are usually referred to as passive sensors. Duan et al. [9] and Chen and Tai [10] use monocular vision in order to detect vehicles and roads. Moreover, [11] combine features and classifiers for vehicle detection. Most of the reported works in obstacle avoidance use stereo cameras to obtain the disparity maps [12, 13], and to obtain the occupancy grids [14]. Seki and Okutomi [15] proposes to extract the road region by estimating the homography matrix between stereo images, [16] detects obstacles by means of the "v-disparity" image and [17] represents the road surface as a general B-spline curve. The method in [18] uses the Sum of Absolute Differences between images meanwhile [19] uses the time-to-impact to objects in the scene to determine free-space. To establish a path to guide a robot, [20] processes the disparity map and then provides a measure for the cost of traversal (Travel Cost Map), choosing the path which has the least associate cost. For free space computation, [21] applies a distance dependent threshold to depth maps, meanwhile [22] and [23] use occupancy grids and its likelihood to be occupied or not. Other approaches also use multi-cameras system for obstacle avoidance [24, 25]. On the other hand, in order to save costs, some references use a single-camera to obtain stereo images using optical systems [26].

Also, many related works combine information from active and passive sensors to improve robustness. Wang et al. [27] acquires information from a single-camera and an odometer; [28] combines a CCD camera with ultrasonic sensors; [29, 30] and [31] use information from a Lidar and a mono-camera for pedestrian, vehicle and object detection respectively; [32] performs an object tracking and obstacle avoidance method using both stereo vision and a laser sensor and [33] combines sonar and range measurements from uncalibrated cameras to help a robot to navigate in an indoor environment.

This paper presents an algorithm for the detection of obstacle-free pathways in real-time, which is integrated in the Cognitive Aid System for Blind and Partially Sighted People (CASBliP) project (http://www.casblip.com). The main aim of CASBliP is to develop a system capable of interpreting and managing real world information from different sources to support mobility-assistance to any kind of visually impaired users. This way, it assists the users to navigate their way outdoors along pavements. There are also several works whose aim is to help people in their navigation, by means of using GPS [34], detecting doorways [35], crosswalks and staircases [36] or the obstacles in the scene [37]. The difference between CASBliP Project and other references which also relay scene information to the blind user (as [38]) lies in the portability of the system. In CASBliP, the device works onboard the visually impaired person. Thus, stereo cameras are constantly moving and the scene often contains blurred and deformed objects. CASBliP also comprises a CMOS time-of-flight sensor to acquire distance information of the immediate range objects.

The motivation of this work is the necessity of detecting surrounding obstacle-free space in real-time to assist in navigation applications. The proposed method presented in this paper introduces the innovation of using depth maps, obtained by the stereovision system, to detect the surrounding obstacle-free space by matching with a linear model.

The paper is organized as follows. The system where the proposed algorithm is included is described in Section 2. The proposed method for obstacle-free pathway detection is detailed in Section 3. Section 4 presents experimental results and, finally, conclusions are drawn in Section 5.

2 Depth Map Extraction

The stereo-vision system comprises two Firewire CCD stereo cameras providing 240×320 pixel images which are calibrated so that estimated internal and external parameters are used to rectify the acquired images. Correspondence between left and right images is followed by disparity and depth estimation. In [39] existing methods to estimate disparity maps are compared and their performance is evaluated with different experiments with indoor images. We have chosen the approach described in [40] to estimate depth maps from from each pair of stereo images. This method is based on dynamic programming and it provides a good trade-off between computational efficiency (about 8–10 depth maps per second) and quality of results. According to [40], depth maps are represented as $N \times M$ gray-scale images where the gray level of each pixel is associated with its nearness. Hence, darker depth map areas are associated to further regions of the scene. The performance of the depth map algorithm is illustrated in Fig. 1, where we show two examples of stereovision images and the corresponding depth maps computed.

Fig. 1 Two examples of stereo images and depth maps. *Left* and *right* images are shown in first and second columns, respectively and third shows the corresponding depth maps computed using [40]

Faster vehicles need to explore and analyze larger distances and areas in the scene. In our case, the algorithm presented in this paper will be used to assist visually impaired people, so we can save running time and computation cost by reducing the number of rows to be analyzed in each depth map.

In a stereo-vision system, distance to objects (Z) is given by [41]:

$$Z = \frac{f * B}{d} \tag{1}$$

where f is the focal length, B is the distance between stereo-cameras and d is the disparity between stereo-images. Bohannon [42] establishes reference values for comfortable walking speed of adults. The mean speed for men aged between 20 and 79 years is 1.39 m/s, so it would be necessary to analyze the next 2.5 m of the scene each second to walk through without the need to stop.

We propose to determine obstacle-free areas by processing only the 25% last rows of the depth maps (from row $N - N/4$ to row N), since these rows represent the scenario region that the user will first walk through. For our depth maps, using Eq. 1 these rows correspond to distances of up to 2.72 m in case of an obstacle-free area. The system works in real-time, providing information at 8 frames per second, which is enough to assist the blind user in the perception of the outdoor environment.

3 Obstacle-Free Pathway Detection

Most of the reported works in obstacle detection use images from a stereo-vision system, since the use of stereo cameras allows the calculation of depth for each pixel in every frame, which is a key feature to perform an accurate detection. Depth maps are calculated from image pixels disparity. The disparity of an image pixel refers the location difference between the pixel in the left image and the corresponding pixel in the right image. Clearly, the lower the disparity for a pixel is, the higher the distance up to the point represented by this pixel.

The detection algorithm presented in this paper is based on the fact that depth map grey levels in obstacle-free areas decrease slightly and linearly from the bottom of the image to the top. On the other hand, obstacles for which depth is approximately constant are represented by flat zones. Figure 2 illustrates this behaviour.

Given a left image I_L and a right image I_R from a stereo-vision system, the depth computed using [40] for pixel in $(row, column)$ location (i, j) is denoted by $D(i, j)$. In order to save computation time and also to reduce the influence of present noise, we process the depth maps by averaging groups of G pixel columns. Thus, we obtain the averaged column $\widetilde{D}(i,k)$ from the values of columns $D(i, j)$, $j = G * k - (G - 1), G * k - (G - 2), G * k - (G - 3), \ldots, G * k$ where $i = N, N - 1, ..., N - N/4$ and $k = 1, 2, ..., M/G$. Then, a least-squares fitting over $\widetilde{D}(i,k)$ is done to find the best linear fitting to adjust the averaged column points. This model, which provides an estimate for $\widetilde{D}(i,k)$, is given by:

$$\hat{D}(i,k) = a_k i + b_k \tag{2}$$

where i is the row number in the processed column of the depth map, $\hat{D}(i,k)$ is the estimated depth, a_k is the gradient and b_k is the y-intercept of the linear

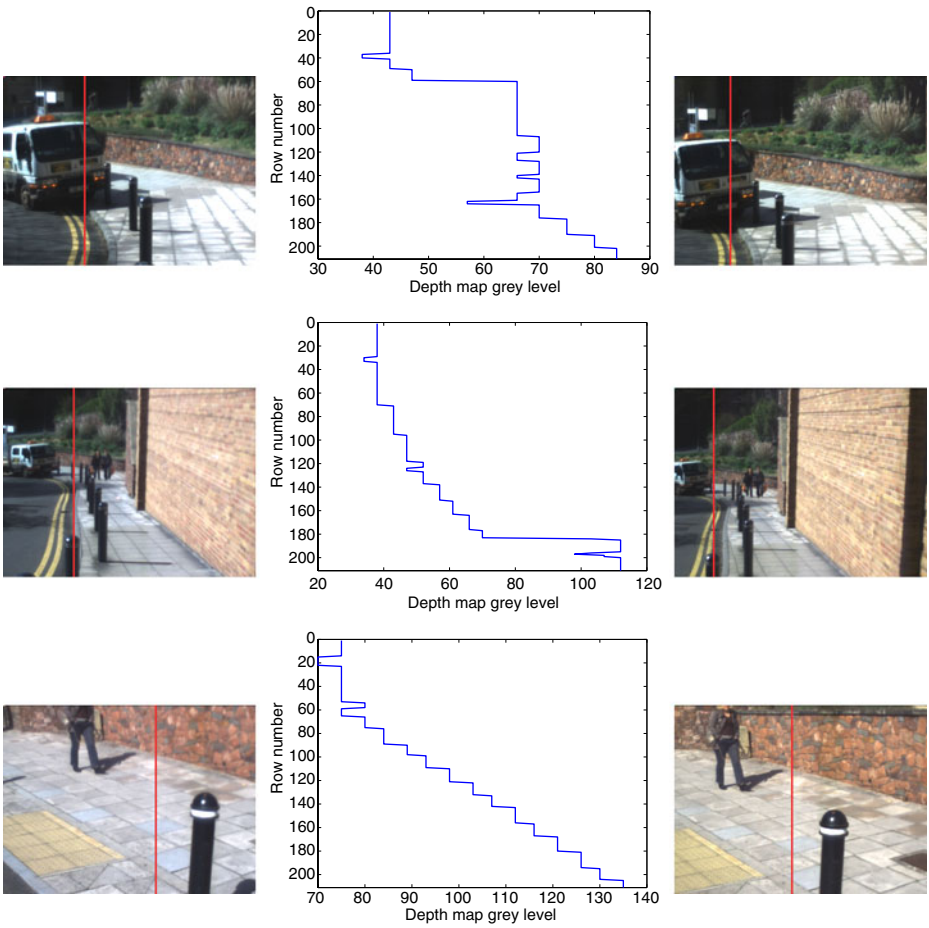

Fig. 2 Three examples to depict the basic principle of the detection method. *First column* Left images from the stereo-vision system. *Second column* Depth map grey levels for the column images marked in the left and right stereo images. *Third column* Right stereo images. In obstacle-free areas (rows from 110 on (first example), rows from 70 to 190 (second example) and rows from 55 on (third example)) grey levels decrease linearly along the column, from the bottom of the image to the top of it. Obstacles (the van, the poles and the wall in these examples) are represented with nearly constant grey values, with variations that do not match our linear model, due to the noise of the depth map

model. Regarding the obtained fitting, its coefficient of determination [43] is defined as

$$I(k) = \frac{\sum_{i=N}^{N-N/4}(\hat{D}(i,k) - \overline{D})^2}{\sum_{i=N}^{N-N/4}(\widetilde{D}(i,k) - \overline{D})^2}, \tag{3}$$

where $\overline{D}$ denotes the mean of the values in $\widetilde{D}(i,k)$. $I(k)$ measures the goodness of the fit for the group of columns $D(i,j)$, $j = G*k-(G-1), G*k-(G-2), G*k-(G-3), \ldots, G*k$. $I(k)$ may take values in [0, 1], where 0 means no correlation and 1 indicates a perfect correlation. According to above, we will determine as

obstacle-free pathways only those groups of columns for which we obtain a good adjustment to the linear model. This implies to require a minimum value $I(k) > I_T$ for considering the candidate group of columns $D(i,j)$, $j = G*k-(G-1), G*k-(G-2), G*k-(G-3), \ldots, G*k$ as an obstacle-free pathway. Also, according to our linear model, depth map grey level in obstacle-free pathways should be decreasing from the bottom of the column to the top. So, we also require that the value of the gradient a_k should be lower than a negative threshold a_T. Furthermore, it is also necessary to establish a threshold b_T for the value b_k, since very near objects can fulfill the requirements for the correlation index I_T and the gradient a_T, but they have high values of b_k. The use of the threshold b_T avoids the possible wrong detection of very near objects as obstacle-free pathways. Algorithm 1 details the proposed detection algorithm.

Algorithm 1: Proposed obstacle-free pathway detection algorithm

```
1  The image is partitioned into disjoint groups of G columns;
2  foreach disjoint group of G columns in the image do
3  |   Compute the averaged column D̃(i,k);
4  |   Adjust the parameters of the linear model D̂(i,k) by LMS (2);
5  |   Compute the value of I(k) (3);
6  |   if I(k) > I_T and a_k < a_T and b_k < b_T then
7  |   |   D(i,j), i = N,N−1,...,N−4, j = G*k−(G−1),G*k−(G−2),G*k−(G−3),...,G*k
   |   |   are marked as an obstacle-free pathway;
8  |   else
9  |   |   D(i,j), i = N,N−1,...,N−4, j = G*k−(G−1),G*k−(G−2),G*k−(G−3),...,G*k
   |   |   are marked as an obstacle;
10 |   end
11 end
```

3.1 Computational Analysis

Regarding the fact that the method has to work in real-time, an analysis of the computation cost has been made. Table 1 shows the result of processing a $N \times M$ pixels depth map (in fact, just the 25% last rows of the depth map—i.e. N/4—have been processed, according to the proposed algorithm). In our case, for $G = 4$, $N = 211$ and $M = 293$, it is necessary to compute 61,823 sums and 50,231 products.

The method has been implemented in C programming language. Under an ACER 5612 at 1.73 GHz it spends 80 ms to obtain the depth map and less than 40 ms to perform the obstacle-free pathway detection, so it is suitable for real-time processes, running at a rate of around 8 frames per second.

Table 1 Number of required operations by processed depth map

	Sums	Products
Columns average	$\frac{N\times M(G-1)}{4G}$	$\frac{N\times M}{4\times G}$
Least minimum squares	$\frac{9\times N\times M}{4\times G}$	$\frac{5\times N\times M}{2\times G}$
Correlation index	$\frac{N\times M}{G}$	$\frac{N\times M}{2\times G}$
Total	$\frac{N\times M(G+12)}{4\times G}$	$\frac{13\times N\times M}{4\times G}$

4 Experimental Results

In order to measure the detection algorithm performance in an objective way, it was necessary to manually prepare some groundtruth images, in which each pixel was marked as free-space or occupied by some object. This way, the detected areas can be compared with the groundtruth images pixel by pixel in order to obtain objective measurements for the detection in terms of True Positives, True Negatives, False Positives and False Negatives. True Positives are defined as the pixels which have been detected as free-space and they really are. True Negatives are the pixels correctly classified as occupied. False Positives are defined as the pixels incorrectly classified as free-space. False Negatives are the pixels which really are free-space, but have been classified as occupied.

We have adjusted the parameters settings involved in the algorithm in order to maximize correct detections and to avoid having False Positives and False Negatives although, due to the application of this detection algorithm, it is more important not to have False Positives than to have False Negatives, in order to avoid collisions with obstacles in the scene. Precision (Eq. 5) is the proportion of true results (True Positives) for all pixels detected. Accuracy (Eq. 6) is the proportion of correct detections (both True Positives and True Negatives) in the tests. Thus, we measure the performance of the method by these parameters by defining a new statistic that we name PACC given by

$$PACC = \frac{Precision + Accuracy}{2}, \tag{4}$$

where

$$Precision = \frac{True\ Positives}{True\ Positives + False\ Positives}, \tag{5}$$

and

$$Accuracy = \frac{True\ Positives + True\ Negatives}{True\ Positives + True\ Negatives + False\ Positives + False\ Negatives} \tag{6}$$

4.1 Parameters Adjustment

A training set of 35 real outdoor images and their corresponding groundtruths have been used to obtain appropriate settings for the algorithm detection parameters. This set includes the most common scenarios that a person can run into outdoors (cars, obstacle-free pathways, pedestrians, walls, poles...) in different illuminating conditions (sunny and cloudy days, shadows of surrounding objects...). This has been necessary since the quality of depth maps used for the detection depends on the illumination conditions of the scene and, as a result, this affects our algorithm, owing to the fact that it is based on the analysis of depth maps. Non-ideally illumination conditions lead the stereo correspondence algorithms to false-matches. Depth maps are less noisy when the scene is well illuminated, since edges in the image are sharper and it is easier to find the disparity between the left and right images from the stereo-vision system. Figure 3 shows a subset of 15 images from the training set.

It is very important to optimize the algorithm parameters in order to maximize the performance that we measure in terms of PACC. Also, it is desirable to have

settings for the parameters that allow the method to perform well for a variety of outdoor images. For this reason, instead of obtaining the optimal values for each image in the training set, we have found the suboptimal values of G, I_T, a_T and b_T that maximize the average of PACC performance for the whole training set. The parameters adjustment of G, I_T, a_T and b_T has been done in an iterative way. Thus,

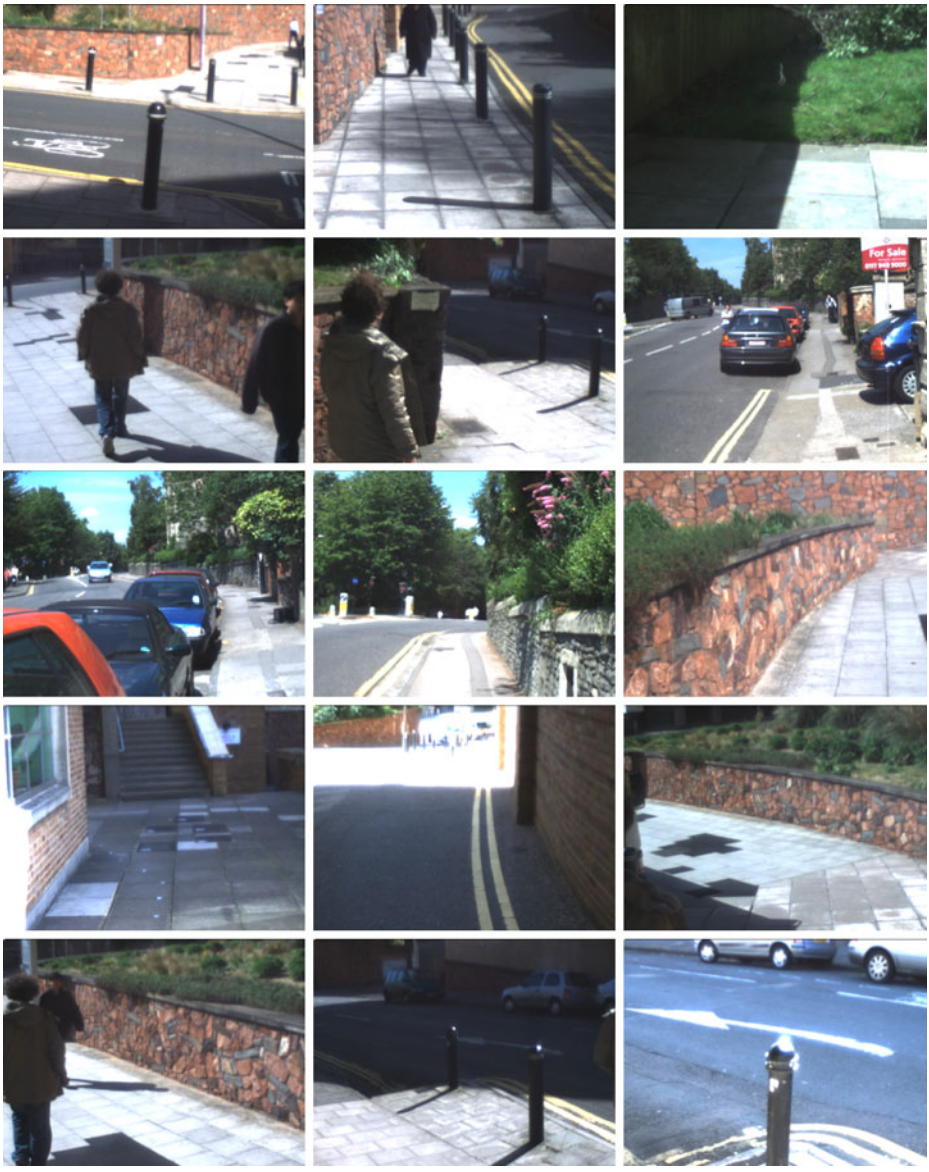

Fig. 3 Subset of 15 images from the left stereo camera of the training set (35 images in total) used for the algorithm's parameters adjustment

once one parameter has been optimized it is fixed, and we proceed to optimize the rest, repeating iteratively until convergence is reached.

In Fig. 4a we can observe the mean PACC performance obtained for the whole training set when the disjoint groups of G columns to be fitted by Least-Mean Squares are varying from 1 to 15, in steps of 1. We can see that we obtain a maximum peak of PACC when $G = 4$ (this is a balance value to average columns in order to reduce the presence of noise but with no loss of the scene information). Figure 4b shows the mean PACC performance obtained for the whole training set as a function of I_T varying from 0.25 to 0.99, in steps of 0.01 where we set $a_T = -0.2$ and $b_T = 150$. We can see that the maximum mean PACC (0.84) is obtained when $I_T = 0.4$ approximately, so we choose this setting for I_T. In Fig. 4c we can see the mean PACC performance obtained for the whole training set as a function of a_T varying from -3 to 1, in steps of 0.01, where we set $I_T = 0.4$ and $b_T = 150$. In this case, the suboptimal setting chosen is $a_T = -0.2$. Figure 4d shows the mean PACC performance when the threshold b_T is varied between 120 and 180. It was necessary to set this threshold to avoid having False Positives in scenes including objects having linear-like decreasing variations in their shape (as car bonnets, for instance). We can see in Fig. 4d that

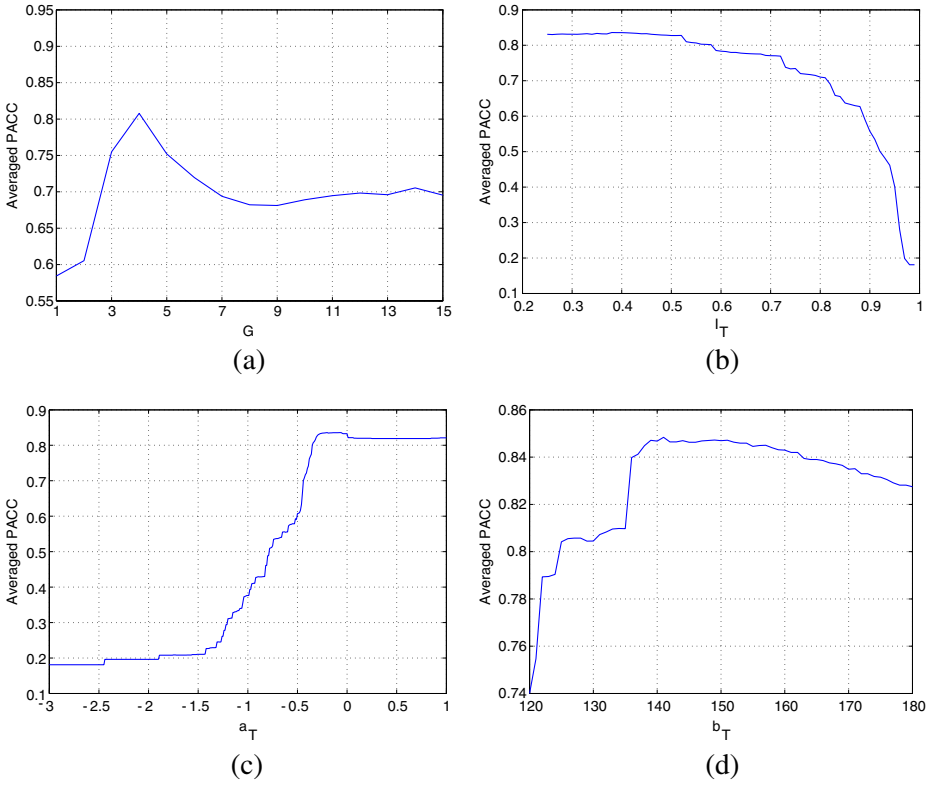

Fig. 4 Averaged PACC: **a** obtained varying the number of averaged columns G, **b** obtained varying correlation threshold I_T, **c** obtained varying gradient threshold a_T, and **d** obtained varying y-intercept threshold b_T. Optimal parameters have been obtained using the whole training set of 35 groundtruth images

Table 2 Performances of the detection method for the training image set

	Precision	Accuracy	PACC
Average	0.9315	0.7624	0.8470
Minimum	0.7771	0.3469	0.6049
Maximum	1	0.9894	0.9897

the optimal value for this threshold is $b_T = 150$, approximately, obtaining in this case about 84% of performance in terms of PACC.

4.2 Algorithm Performance

In this section we assess the performance of the obstacle-free pathway detection method, using the previous suboptimal settings for G, I_T, a_T and b_T. Table 2 shows that the average of the PACC values in processed training images set is about 84%. It is very important to note that mean Precision value is about 93%. This happens because the detection algorithm maximizes True Positives, which have a high influence in the Precision statistic. Also, notice that this fact supports the suitability of the developed method for our application where, as commented above, it is very important to maximize True Positives. However, since Accuracy also depends on True Negatives, its mean value is a little lower. As we have explained before, for our application it is more important not to have False Positives than to have False Negatives in order to avoid having collisions, so the method performs appropriately.

Table 3 shows the performance for a testing image set, which is shown in Fig. 5. These figures confirm that the algorithm works and detects obstacle-free pathways properly, with performance about 83% in terms of PACC percentage. Moreover, Tables 4 and 5 show the detection performance for favorable scenarios (well illuminated scenes, no shadows, textures images) and less favorable scenarios (bad lightning, shadows, no texture), respectively. We observe that there are images for which Precision is very high since almost all obstacle-free areas detected are correct (Fig. 5b, d, i–k). On the other hand, we also observe that Accuracy is low because a few free-paths are missed. Usually, they correspond to borders of the image or corners (Fig. 5a), untextured scene areas that can not be matched between left and right stereoimages (Fig. 5e, h, l, w, x), very noisy zones of depth maps (Fig. 5c) or not well illuminated zones (Fig. 5d, g, o, q, r, t). Besides, we have shown also Recall figures (Eq. 7) for the testing image set, in order to show how the False Negatives affect to it. Bad illumination conditions reduce this performance about 34%.

$$Recall = \frac{True\ Positives}{True\ Positives + False\ Negatives}, \tag{7}$$

Nevertheless, detections are accurate: we can see that in all cases we can detect the wider free space area to walk through, so the method performs appropriately for the

Table 3 Performances of the detection method for the testing image set

	Precision	Accuracy	PACC	Recall
Average	0.9565	0.7077	0.8321	0.6301
Minimum	0.6441	0.3517	0.63675	0.3517
Maximum	1	0.9561	0.9705	0.9269

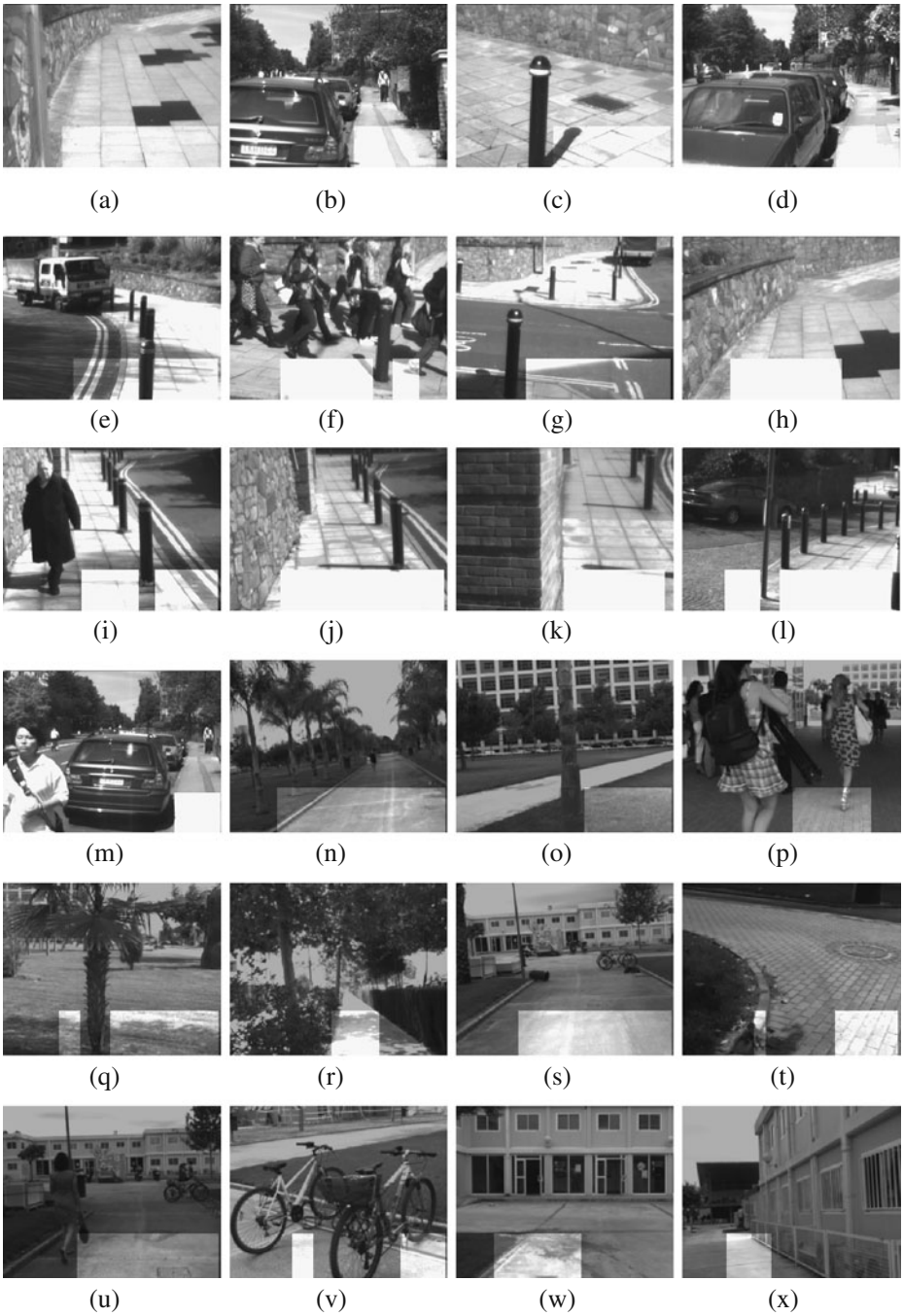

Fig. 5 Processed testing images set. Brighter areas show detected obstacle-free pathways. The visual analysis reveals that sometimes obstacle-free areas are not detected. Usually, they correspond to borders of the image or corners (**a**); untextured scenes—areas that can not be matched between *left* and *right* stereoimages—(**e**, **h**, **l**, **w**, **x**); very noisy zones of depth maps (**c**) or not well illuminated zones (**d**, **g**, **o**, **q**, **r**, **t**)

Table 4 Performances of the detection method for favorable scenarios of the testing image set

	Precision	Accuracy	PACC	Recall
Average	0.9842	0.8247	0.8990	0.7713
Minimum	0.9076	0.5726	0.7645	0.5689
Maximum	1	0.9561	0.9705	0.9269

Table 5 Performances of the detection method for less favorable scenarios of the testing image set

	Precision	Accuracy	PACC	Recall
Average	0.9305	0.5887	0.7507	0.5090
Minimum	0.6441	0.3517	0.6368	0.3517
Maximum	1	0.7228	0.8614	0.7060

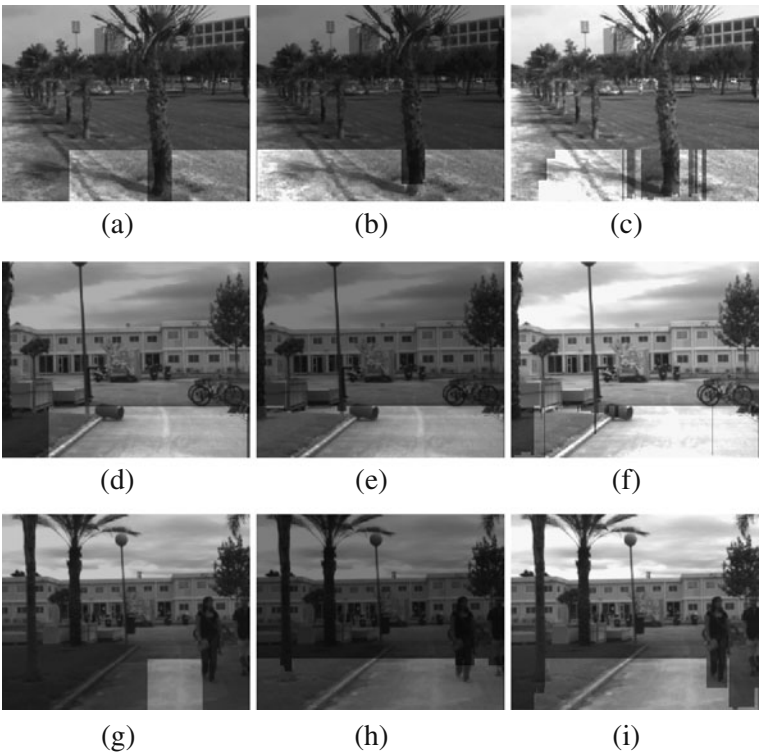

Fig. 6 Examples of testing images set. Brighter areas show detected obstacle-free pathways. *First column* shows results of the proposed method, *second column* shows [44] results and *third column* shows [22] results

Table 6 Performances for the testing image set

	Our method	[44]	[22]
Precision	0.9565	0.9557	0.9779
Accuracy	0.7077	0.9548	0.8054
Recall	0.6301	0.9989	0.8151
PACC	0.8321	0.9552	0.8917

purpose of the project in which it is integrated. There are also no obstacles detected as free space, and collisions are avoided.

Finally, we have compared the detection results of our method with another two recent references [22] and [44]. Figure 6 shows three different detection results examples for the three methods. We can see that the algorithm avoids the obstacles in the scene and that it always detects the wider obstacle-free pathway to walk through. Table 6 shows the performance of the three methods for the testing set. As we have explained before, for our application it is more important not to have False Positives than to have False Negatives in order to avoid having collisions, although sometimes it leads to have some False Negatives. Thus, maximizing True Positives means to maximize Precision. We can observe that our method obtains similar values of Precision compared with the other two references. It confirms that the algorithm works and detects free paths properly. Moreover, our algorithm is suitable for working in real-time and more efficient computationally, which is essential to be integrated as a support to navigate for visually impaired people.

5 Conclusions and Future Work

In this paper we have presented a new method for obstacle-free pathway detection which is based on an analysis of depth maps obtained from processing a pair of stereoimages. The method is based on detecting as obstacle-free areas the depth map columns that match a linear model. For this, the best first-degree polynomial adjusting the cloud of points is obtained by the least-squares method and the obtained result is checked to meet the desired requirements. Computational analysis of the method has been done to assess its suitability for real-time processing. An experimental study has been used to derive suboptimal settings for the method parameters. Experimental results on real outdoor images show that the method provides good results. Future work could focus on improving the algorithm performance in the presence of non-ideal lightning conditions (for example, Fig. 5l and o) and in areas where it is difficult to match left and right stereoimages, since texture is missing in some areas of the scene (for example, Fig. 5e and w). In addition, the next step of this work may include temporal coherence to track the obstacle-free pathways and perform a continuous detection.

References

1. Huang, Y., Fu, S., Thompson, C.: Stereovision-based object segmentation for automotive applications. EURASIP J. Appl. Signal Process. **2005**(14), 2322–2329 (2005)
2. Bertozzi, M., Broggi, A.: Gold: a parallel real-time stereo vision system for generic obstacle and lane detection. IEEE Trans. Image Process. **7**(1), 62–81 (1998)
3. Sun, Z., Bebis, G., Miller, R.: On-road vehicle detection: a review. IEEE Trans. Pattern Anal. Mach. Intell. **28**(5), 694–711 (2006)
4. Blanco, J.L., Gonzalez, J., Fernandez-Madrigal, J.A.: Exteding obstacle avoidance methods through multiple parameter-space transformations. Auton. Robots **24**(1), 29–48 (2008)
5. Lindner, P., Wanielik, G.: 3d lidar processing for vehicle safety and environment recognition. In: IEEE Workshop on Computational Intelligence in Vehicles and Vehicular Systems, pp. 66–71. IEEE (2009)

6. Dolgov, D., Thrun, S.: Autonomous driving in semi-structured environments: mapping and planning. In: International IEEE Conference on Robotics and Automation, pp. 3407–3414. IEEE (2009)
7. Hernandez, A., Ureña, J., Mazo, M., Garcia, J.J., Jimenez, A., Jimenez, J.A., Perez, M.C., Alvarez, F.J., De Marziani, C., Derutin, J.P., Serot, J.: Advanced adaptive sonar for mapping applications. J. Intell. Robot. Syst. **55**(1), 81–106 (2009)
8. Del Castillo, G., Skaar, S., Cardenas, A., Fehr, L.: A sonar approach to obstacle detection for a vision-based autonomous wheelchair. Robot. Auton. Syst. **54**(12), 967–981 (2006)
9. Duan, B.B., Liu, W., Fu, P.Y., Yang, C.Y., Wen, X.Z., Yuan, H.: Real-time on-road vehicle and motorcycle detection using a single camera. In: IEEE International Conference on Industrial Technology, pp. 579–584. IEEE (2009)
10. Chen, C., Tai, C.: Adaptive fuzzy color segmentation with neural network for road detections. Eng. Appl. Artif. Intell. (2009). doi:10.1016/j.engappai.2009.12.004
11. Oliveira, L., Nunes, U.: On integration of features and classifiers for robust vehicle detection. In: IEEE International Conference on Intelligent Transportation Systems, pp. 414–419. IEEE (2008)
12. Nalpantidis, L., Kostavelis, I., Gasteratos, A.: Stereovision-based algorithm for obstacle avoidance. In: Lecture Notes in Computer Science. Intelligent Robotics and Applications (2009)
13. Franke, U., Heinrich, S.: Fast obstacle detection for urban traffic situations. IEEE Trans. Intell. Transp. Syst. **3**(3), 173–181 (2002)
14. Murray, D., Little, J.J.: Using real-time stereo vision for mobile robot navigation. Auton. Robots **8**(2), 161–171 (2000)
15. Seki, A., Okutomi, M.: Robust obstacle detection in general road environment based on road extraction and pose estimation. Electron. Commun. Jpn., Part 2, Electron. **90**(12), 12–22 (2007)
16. Labayrade, R., Aubert, D., Tarel, J.P.: Real time obstacle detection in stereo vision on non-flat road geometry through v-disparity representation. In: INRIA. IEEE Intelligent Vehicle Symposium (2002)
17. Wedel, A., Badino, H., Rabe, C., Loose, H., Franke, U., Cremers, D.: B-spline modeling of road surfaces with an application to free-space estimation. IEEE Trans. Intell. Transp. Syst. **10**(4), 572–583 (2009)
18. Nguyen, T.H., Nguyen, J.S., Pham, D.M., Nguyen, H.T.: Real-time obstacle detection for an autonomous wheelchair using stereoscopic cameras. Conf. Proc. IEEE Eng. Med. Biol. Soc. **2007**(1), 4775–4778 (2007)
19. Grosso, E., Tistarelli, M.: Active/dynamic stereo vision. IEEE Trans. Pattern Anal. Mach. Intell. **17**(9), 868–879 (1995)
20. Vergauwen, M., Pollefeys, M., Van Gool, L.: A stereo-vision system for support of planetary surface exploration. Mach. Vis. Appl. **14**(1), 5–14 (2003)
21. Franke, U., Joos, A.: Real-time stereo vision for urban traffic scene understanding. In: IEEE Intelligent Vehicles Symposium. IEEE (2000)
22. Badino, H., Mester, R., Vaudrey, T., Franke, U.: Stereo-based free space computation in complex traffic scenarios. In: IEEE Southwest Symposium on Image Analysis & Interpretation, pp. 189–192 (2008)
23. Badino, H., Franke, U., Mester, R.: Free space computation using stochastic occupancy grids and dynamic programming. In: Workshop on Dynamical Vision, ICCV. Rio de Janeiro, Brazil (2007)
24. Henrich, D., Gecks, T.: Multi-camera collision detection between known and unknown objects. In: IEEE International Conference on Distributed Smart Cameras, pp. 390–399. IEEE (2008)
25. Nalpantidis, L., Chrysostomou, D., Gasteratos, A.: Obtaining reliable depth maps for robotic applications from a quad-camera system. In: International Conference on Intelligent Robotics and Applications. Lecture Notes in Artificial Intelligence, pp. 906–916 (2009)
26. Lovegrove, W., Brame, B.: Single-camera stereo vision for obstacle detection in mobile robots. In: Intelligent Robots and Computer Vision XXV: Algorithms, Techniques and Active Vision, pp. T7640–T7640. Conference on Intelligent Robots and Computer Vision XXV—Algorithms, Techniques, and Active Vision (2007)
27. Wang, H., Yuan, K., Zou, W., Peng, Y.: Real-time region-based obstacle detection with monocular vision. In: International Conference on Robotics and Biomimetics, pp. 615–619. IEEE (2005)
28. Choi, S., Jin, T., Lee, J.: Obstacle avoidance algorithm for visual navigation using ultrasonic sensors and a ccd camera. Artif. Life Robot. **7**(3), 132–135 (2003)
29. Premebida, C., Ludwig, O., Nunes, U.: Lidar and vision-based pedestrian detection system. Journal of Field Robotics **26**(9), 696–711 (2009)

30. Premebida, C., Monteiro, G., Nunes, U., Peixoto, P.: A lidar and vision-based approach for pedestrian and vehicle detection and tracking. In: International IEEE Conference on Intelligent Transportation Systems, pp. 83–88. IEEE (2007)
31. Douillard, B., Fox, D., Ramos, F.: A spatio-temporal probabilistic model for multi-sensor object recognition. In: International Conference on Intelligent Robots and Systems, pp. 2408–2414. IEEE (2007)
32. Tsalatsanis, A., Valavanis, K., Yalcin, A.: Vision based target tracking and collision avoidance for mobile robots. J. Intell. Robot. Syst. **48**(2), 285–304 (2007)
33. Tsalatsanis, A., Valavanis, K., Tsourveloudis, N.: Mobile robot navigation using sonar and range measurements from uncalibrated cameras. J. Intell. Robot. Syst. **48**(2), 253–284 (2007)
34. Loomis, J.M., Golledge, R.G., Klatzky, R.L.: Navigation system for the blind: auditory display modes and guidance. Presence **7**(2), 193–203 (1998)
35. Snaith, M., Lee, D., Probert, P.: A low-cost system using sparse vision for navigation in the urban environment. Image Vis. Comput. **16**(4), 225–233 (1998)
36. Se, S., Brady, M.: Road feature detection and estimation. Mach. Vis. Appl. **14**(3), 157–165 (2003)
37. Molton, N., Se, S., Brady, J.M., Lee, D., Probert, P.: A stereo vision-based aid for the visually impaired. Image Vis. Comput. **16**(4), 251–263 (1998)
38. Picton, P.D., Capp, M.D.: Relaying scene information to the blind via sound using cartoon depth maps. Image Vis. Comput. **26**(4), 570–577 (2008)
39. Scharstein, D., Szeliski, R.: A taxonomy and evaluation of dense two-frame stereo correspondence algorithms. Int. J. Comput. Vis. **47**(1/2/3), 7–42 (2002)
40. Birchfield, S., Tomasi, C.: Depth discontinuities by pixel-to-pixel stereo. Int. J. Comput. Vis. **17**(3), 269–293 (1999)
41. Hartley, R.I., Zisserman, A.: Multiple View Geometry in Computer Vision, 2nd edn. Cambridge University Press. ISBN: 0521540518 (2004)
42. Bohannon, R.W.: Comfortable and maximum walking speed of adults aged 20–79 years: reference values and determinants. Age Ageing **26**(1), 15–19 (1997)
43. Spiegel, M.R., Stepthens, L.J.: Statistics, 4th edn. Mc Graw Hill (2008)
44. Kubota, S., Nakano, T., Okamoto, Y.: A global optimization for real-time on-board stereo obstacle detection systems. In: IEEE Intelligent Vehicles Symposium. IEEE (2007)